JOURNAL OF MATERIALS SCIENCE 17 (1982) 277–289

Fatigue behaviour of metallic fibre-reinforced materials: a study of steel fibre-reinforced silver

Part 2 *Failure mechanisms and high-cycle fatigue life*

G. ROSENKRANZ, V. GEROLD
Max-Planck-Institut für Metallforschung, Institut für Werkstoffwissenschaften, and Institut für Metallkunde, Universität Stuttgart, Federal Republic of Germany

K. KROMP
University of Vienna, Austria

D. STÖCKEL, L. TILLMANN
G. Rau, Pforzheim, Federal Republic of Germany

Fatigue damage and crack propagation modes in composites with unidirectionally aligned fibres may be affected by several variables such as fibre and matrix strength, fibre–matrix interfacial bonding and possible fluctuations in the strength of the reinforcing fibres. The influence of the different parameters on the behaviour of metallic fibre-reinforced materials was investigated up to 10^8 cycles in a model compound of steel-fibre-reinforced silver. The fatigue tests were carried out at a frequency of 20 kHz using an ultrasonic equipment. Two fundamentally different failure mechanisms and several transitional modes have been observed: (a) failure by nucleation and propagation, usually of one matrix fatigue crack, with simultaneous failure of the reinforcing fibres, (b) failure by gradual accumulation of matrix and interface fatigue damage and fibre-inhibited propagation of the final fatigue crack. The occurrence of both mechanisms depends mainly on the development of the local stress conditions when a matrix fatigue crack is approaching a fibre. This is discussed in terms of a simple model. Additionally, the effect of the failure mechanism on fatigue life and on the design of an appropriate failure criterion is considered.

1. Introduction

The low-cycle fatigue behaviour of silver–steel-fibre-reinforced composites (FRC) with constant fibre volume-fraction, $V_f = 0.35$ was considered in Part 1 of this study [1]. It was reported that variations of the fibre and matrix strengths, as well as the fibre–matrix interfacial bond, gain increasing significance for the fatigue damage and failure mechanisms if the stress or total strain amplitude is decreased. The present paper demonstrates the influences on damage and failure mechanisms, especially at high-cycle fatigue (numbers of cycles to failure 10^6 to 10^8), on the basis of experimental results and a qualitative model. Additionally, the effect of different fatigue failure modes on fatigue life and the choice of an appropriate failure criterion will be discussed.

Fatigue testing was carried out using the same silver–steel FRCs and, for comparison, unreinforced silver samples, as in Part 1 [1]. Because of the relatively little effect of fibre diameters (in the range from approximately 35 μm to 200 μm)

0022–2461/82/010277–13$03.30/0

on the interesting fatigue mechanisms, only the results of composites with 200 μm filaments will be presented in this study.

As in Part 1, the following sample conditions were investigated: two sets of specimens were manufactured; one set had been 30% cold-worked and the other 80% cold-worked by the drawing process. These sets are named 30/D and 80/D, respectively, for convenience. Some specimens were annealed in an inert atmosphere in order to recrystallize the matrix (30/R and 80/R, respectively), others were given an annealing treatment in an oxidizing atmosphere (30/Ox and 80/Ox, respectively) in order to recrystallize the matrix and oxidize the fibre surfaces.

2. Experimental method

An ultrasonic fatigue testing method, which has been described in more detail elsewhere [2], was used for the high-cycle fatigue tests of both the silver–steel composites and the unreinforced silver. The samples were excited to symmetric longitudinal vibrations of 20 ± 2 kHz. The vibration energy was fed to both ends of the specimens by piezoelastic transducers (nominal power 1 kW), an acoustic transformer and suitable coupling pieces. For further increase of the achievable total-strain amplitude, dumb-bell-shaped samples with a 6 mm gauge length and 3 mm diameter were fabricated from as-received rods. This particular specimen shape has surfaces composed of longitudinally cut filaments embedded in the silver matrix. The constant total-strain amplitude ($\Delta\epsilon_{tot} = 2.8$ to 4×10^{-3}) was directly registered by mounted minature strain gauges (Hottinger–Baldwin Ly 11) in the centre of the specimen gauge length. For calibration of the strain gauges a resonant system with minimum damping was used by substituting the sample by a coupling piece made of a Ti–6 wt% Al–4 wt% V alloy. From the widening of a light marker in a maximum of motion of the system it is possible to calculate the maximum strain in the centre of the gauge length, i.e. where the strain gauge is located. A direct measurement of the cyclic stress amplitude is not possible in ultrasonic fatigue tests.

In order to reduce heating of the sample during cycling, two precautions were taken. Firstly, a coolant oil was ejected radially on to the centre part of the specimen. Secondly, the following pulse technique was used: the material was fatigued by a wave packet containing a controllable number of ultrasonic vibrations (2000–3000 cycles). After a pause of controllable length (5000–20 000 cycles) the next wave packet was imposed, and so on. Under some sample conditions the damping behaviour of the material varied greatly during fatigue testing; this caused a shift of the test frequency and finally led to the loss of resonance. This moment was defined as a failure criterion irrespective of the stage of damage in different materials (see Section 4.3).

The frequency effect, i.e. differences between high- and low-frequency fatigue, has been studied by several groups in the past. As a rule, an increase in the number of cycles to failure with increasing test frequency has been reported [3]. In the present study, however, observed tendencies of fatigue damage development and failure mechanisms for different material conditions in low-frequency, i.e., low-cycle fatigue, tests [1], suggested that the fundamental fatigue response of the composites was independent of the test frequency. Hence, it may be assumed that fatigue lives found in high-frequency tests may indeed differ from low-frequency measurements, but that the relative changes in behaviour of samples with different material conditions are not essentially influenced by the use of the ultrasonic fatigue testing method.

3. Experimental results

3.1. Fatigue damage and failure

Fatigue damage and failure mechanisms of different silver–steel FRCs were observed during test interruptions and after failure by scanning electron microscopy (SEM) investigations of fracture surfaces and longitudinal sections.

3.1.1. 30% pre-deformed composites (30/D 30/R and 30/Ox conditions)

Irrespective of the total strain amplitude, 30% pre-deformed composites without further heat treatment (30/D) show a macroscopically flat fatigue fracture surface with low steps only. After formation of some visible fatigue cracks at the specimen surface, only one of them propagates into the bulk material and induces fatigue cracks in the filaments whenever meeting with a fibre–matrix interface. The SEM micrograph (Fig. 1a) of a fracture surface section of a sample with $N_f = 1.33 \times 10^5$ cycles confirms this behaviour on a microscopic scale. Lines of rest, which cross the fibre–matrix interface without any change of direction also indicate the incapability of the

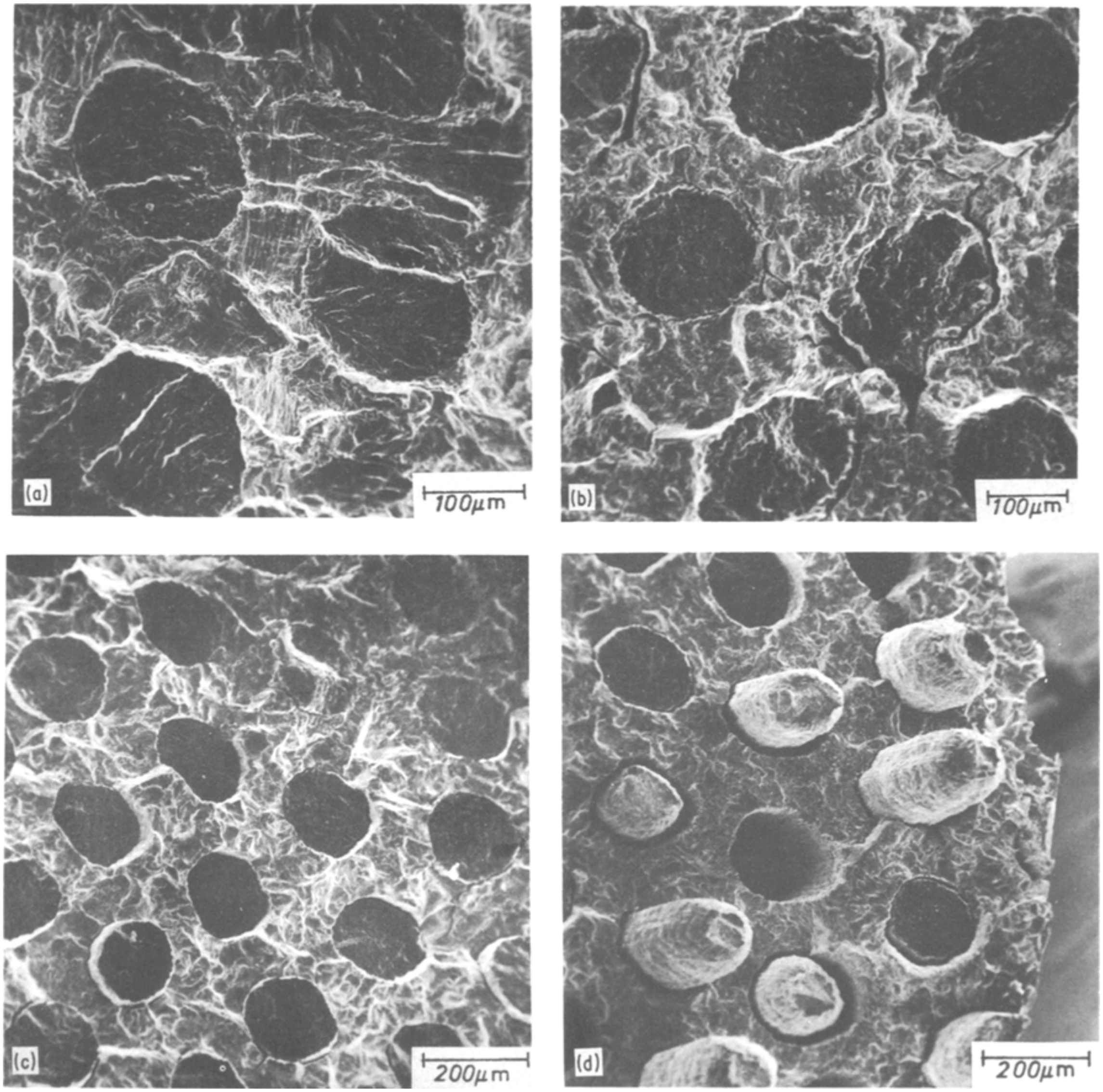

Figure 1 Fatigue fracture surfaces of 30% cold-drawn FRC with different heat treatments ($\Delta\epsilon_{tot} = 0.52\%$). (a) as-received. $N_f = 1.33 \times 10^5$ cycles; (b) matrix recrystallized; $N_f = 6.4 \times 10^4$ cycles; (c) *in situ* oxidized filament surfaces; $N_f = 4 \times 10^4$ cycles; (d) same as (c); pulled-out filaments fractured in a subsequent tensile test.

filaments to impede or stop matrix fatigue crack growth. In the schematic presentation (Fig. 2), which will be repeatedly referred to for comparison and clarification, the actual behaviour corresponds to Case a in Fig. 2.

In the 30/R condition, rest lines as in Fig. 1a can no longer be observed (Fig. 1b). Instead, the macroscopically flat fracture surface shows indications of debonding processes along the fibre–matrix interface (Fig. 2b). An additional *in situ* oxidation of the steel–fibre surfaces (30/Ox condition) leads to a very weak interfacial bond [4] which results in complete delamination and merely mechanical keying of the interface during the fatigue experiment. The fracture surface still remains macroscopically flat, but the SEM micrograph (Fig. 1c) reveals small steps between fractured fibres (dark fracture surfaces) and the matrix fracture plane. Marked pull-outs develop during tensile fracture of the remaining sample cross-section after fatigue failure (Fig. 1d). Furthermore the micrograph shows that, in this material state, fatigue cracks no longer propagate continuously, since some fibres survive uncracked when by-

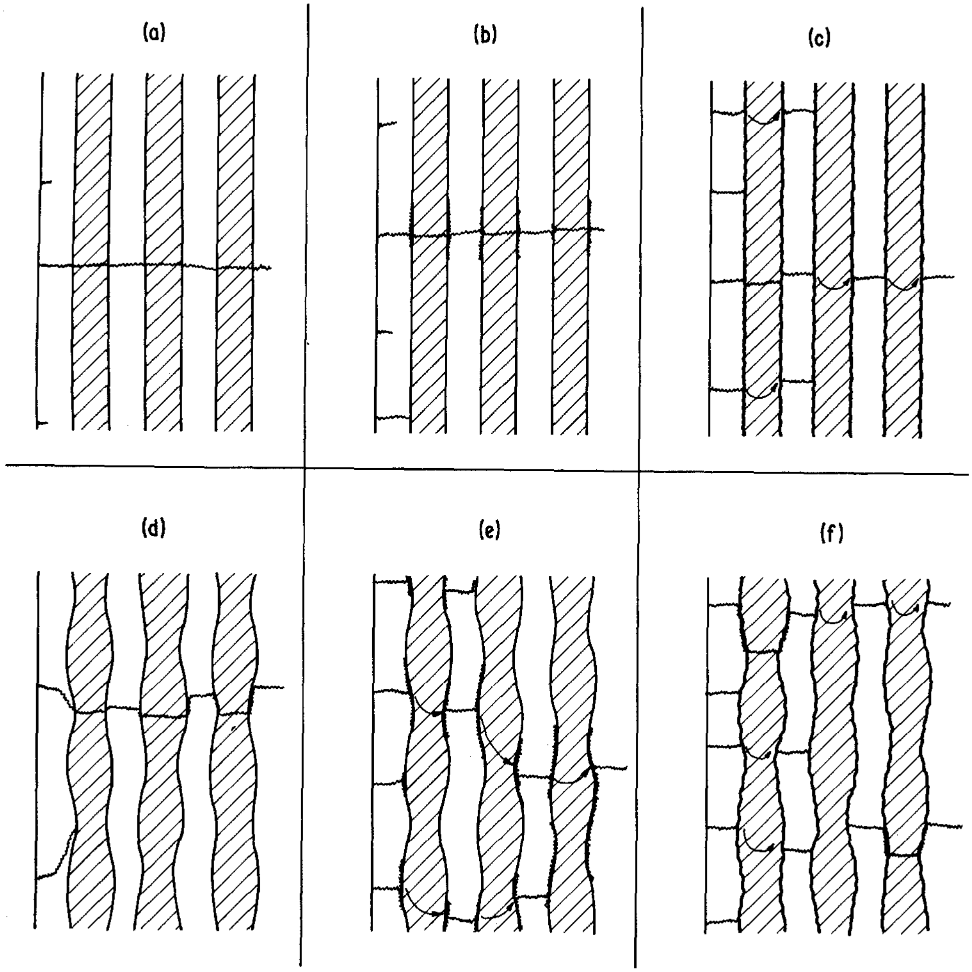

Figure 2 Schematic illustration of important failure modes in differently heat-treated Ag/St FRC near the fatigue limit; specimen surface on the left-hand side of each drawing.

passed by a matrix fatigue crack. This tendency is especially confirmed at low strain amplitudes near the fatigue limit. Several matrix fatigue cracks nucleate at the specimen surface, but fibre damage is not usually found. The longitudinal section (Fig. 3) is taken from a sample which was fatigued 2.4×10^{7} cycles at a total strain amplitude of 3.4×10^{-3} and subsequently fractured in a tensile test. The many matrix fatigue cracks are blunted during the subsequent tensile test and become macroscopically visible. Under this material condition matrix fatigue cracks are obviously unable to propagate into the filaments when they meet a fibre–matrix interface. Nevertheless, matrix damage gradually advances into the bulk of the specimen by by-passing the fibres. A subsequent tensile test after 10^{8} cycles at $\Delta\epsilon_{tot} = 2.8 \times 10^{-3}$ revealed that the matrix cross-section had failed mainly during fatigue, while all fibres failed only afterwards during the tensile test (schematic presentation, Fig. 2c).

3.1.2. 80% pre-deformed composites (80/D, 80/R and 80/Ox conditions)

Fatigue loading of 80% pre-deformed silver–steel FRC partially led to important differences compared with the damage and crack growth behaviour described above. These differences are due to the increased fibre strength and to the specific filament shape (multiple necking) [5].

In the two 80/D and 80/R conditions, an elevated local plastic strain amplitude is induced by the fibre defects in the surrounding matrix zone. During fatigue cycling these highly deformed zones arrange themselves in the form of double-cones around the fibres. On the specimen surface the double-cones appear in an X-shaped manner. These zones are obviously areas of crack nucleation

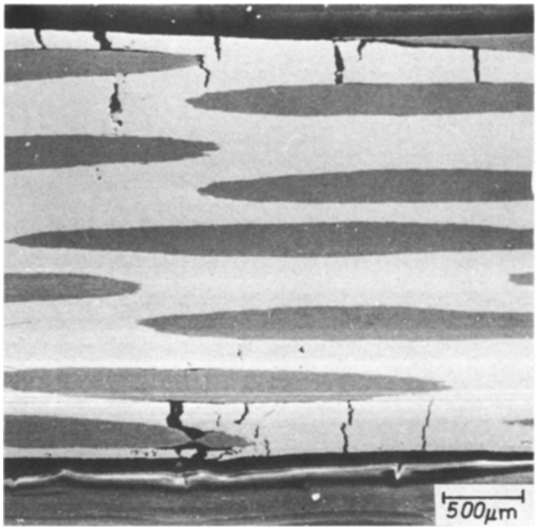

Figure 3 Longitudinal section of a 30% pre-deformed FRC specimen with *in situ* oxidized filament surfaces; $\Delta\epsilon_{tot} = 3.4 \times 10^{-3}$, $N = 2.4 \times 10^{7}$ cycles, fractured in a subsequent tensile test; several matrix fatigue cracks start from the specimen surface but no fibre fatigue damage is observed.

or propagation. As an example the micrograph of Fig. 4 shows a surface section of a sample fatigued to failure at $\Delta\epsilon_{tot} = 5.2 \times 10^{-3}$ ($N_f = 1.65 \times 10^5$ cycles). It was obtained after a low-cycle fatigue test which allowed the *in situ* observation of crack propagation at the surface.

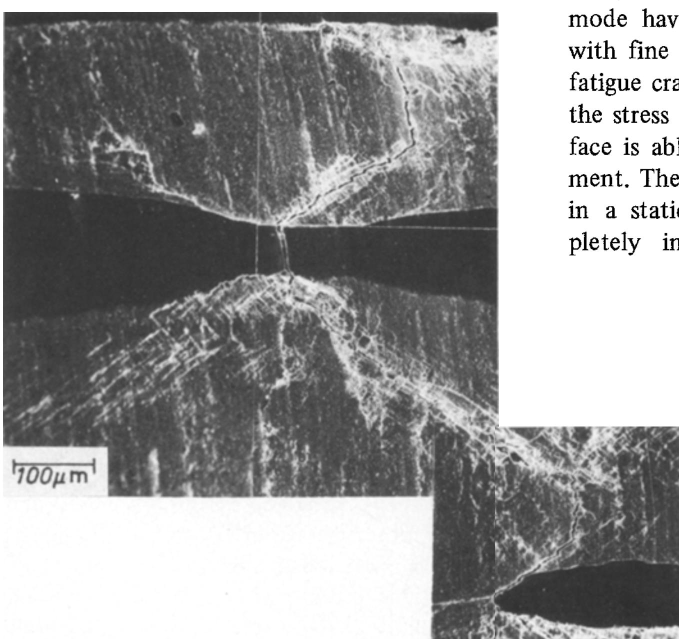

Figure 4 Surface fatigue crack of a 80% cold-drawn FRC specimen; $\Delta\epsilon_{tot} = 0.52\%$, $N_f = 1.65 \times 10^5$ cycles.

After development of the X-shaped deformation zone, the surface fibre failed in the necking region. Subsequently, the crack propagated into the matrix following the deformed zone at an angle of approximately 45° to the fibre. It then bent to a direction perpendicular to the axis and finally by-passed a discontinuity, again at an angle of 45° (see bottom of Fig. 4). In the opposite direction, no severe fibre defect or discontinuity is present to serve as a possible crack path. Consequently, the crack was impeded for some 10^4 cycles, while the matrix deformation obviously increased and crack branching was observed (see top of Fig. 4) before at last a fatigue crack was induced in the filament. Fig. 5a shows a section of a fracture surface of a similar specimen. Contrary to the 30% deformed samples, several fibres fractured above or below the matrix fracture level. But fatigue crack branching along the fibres prior to formation of a fibre crack occurs only in specific cases. Unlike the behaviour at the surface, matrix fatigue cracks in the bulk run either perpendicular to or along the filament axis. The 45° cracks could be observed only at very high strain amplitudes ($\Delta\epsilon_{tot} = 8 \times 10^{-3}$) (Fig. 2d). Fig. 5b demonstrates the ability of the highly deformed steel fibres to impede matrix crack propagation. The micrographs represents the transition from fatigue failure to tensile fracture of the remaining cross-section. Fibres broken during cyclic loading look dark, while those fractured in the static tensile mode have a much lighter appearance associated with fine dimples. As can be seen in Fig. 5b the fatigue crack front bends between the fibres until the stress concentration at the fibre–matrix interface is able to induce a fatigue crack in the filament. The fibre marked by an arrow was fractured in a static tensile manner but lies almost completely in the fatigue fractured matrix zone.

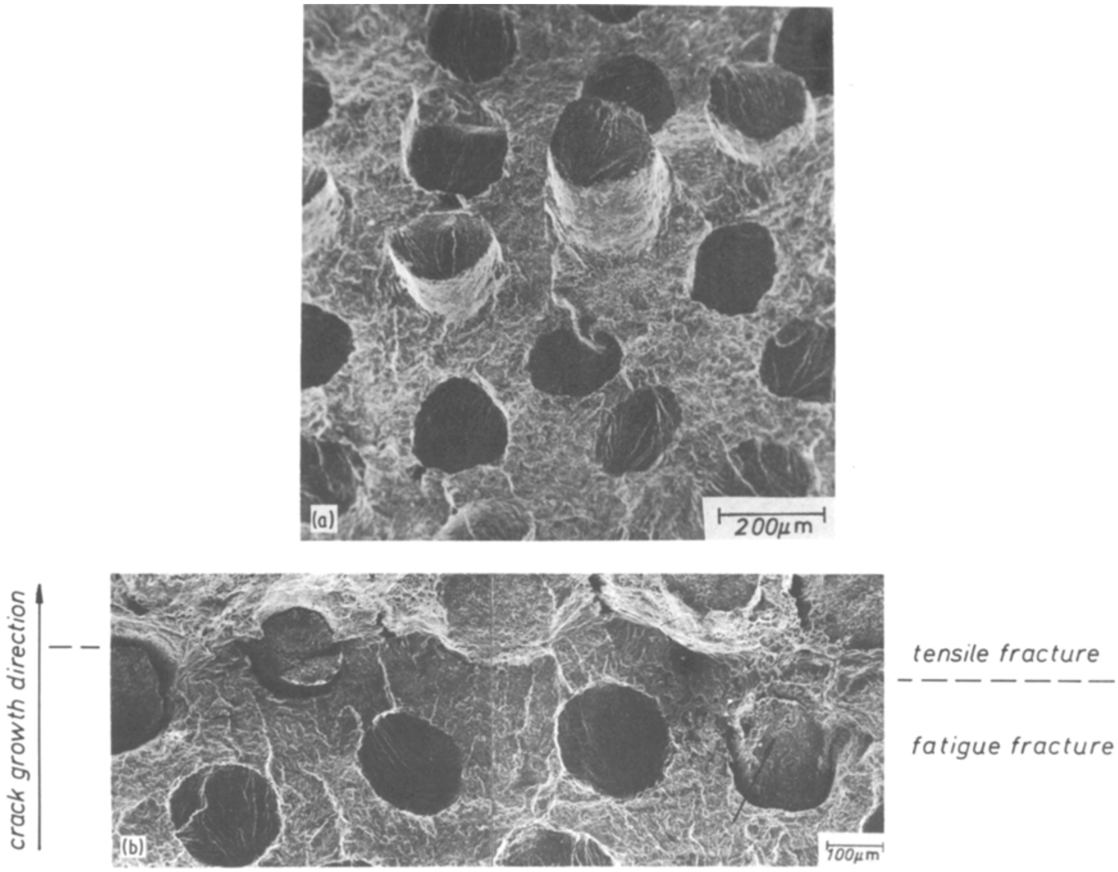

Figure 5 Fatigue fracture surface of a 80% cold-drawn FRC specimen; $\Delta\epsilon_{tot} = 4.0 \times 10^{-3}$, $N_f = 5.4 \times 10^6$ cycles. (a) Some fibres are fractured above the matrix fracture plane and; (b) transition from fatigue to tensile fracture (see text).

After matrix recrystallization (80/R condition) surface damage develops in a similar manner as described above, but matrix cracks inititate much earlier and are more numerous during fatigue under comparable strain amplitudes. On the other hand, matrix crack growth is observed to be much slower than in the as-drawn samples. During low-cycle fatigue, reported in Part 1, the resulting gradual damage accumulation could be followed *in situ* with a stereo-microscope and is, for example, characterized by a slowly decreasing stress amplitude in a strain-controlled test (Part 1, Fig. 6a). Fractographic investigations of the high-cycle specimens reveal that the fibre crack planes do not usually coincide with the matrix crack plane (Fig. 6a). Their failure is generally determined by the position of the fibre neckings. The matrix itself is cut in several planes perpendicular to the loading direction prior to fibre cracking. The association of such cracked zones finally results in several macroscopic steps in the fracture surface. All fibres of a specimen which was cycled to $N = 10^8$ at $\Delta\epsilon_{tot} = 2.8 \times 10^{-3}$ remained unbroken and failed only in a subsequent tensile test (Fig. 6b). The severely pre-deformed filaments often broke in a shear mode at low tensile strains. The matrix, however, was completely or partially separated during fatigue in several parallel planes. A fine structured matrix fracture surface (Fig. 6b) arises from the extraordinarily high number of test cycles compared to the cycle number needed for matrix failure ($\sim 5 \times 10^7$ cycles). A longitudinal section of the same specimen (Fig. 6c) illustrates that the filaments have been by-passed by matrix cracks (Fig. 2e). It should be noted that debonding of the fibre–matrix interface in this material condition is restricted to the zone adjacent to the matrix fatigue crack planes. The cracks do not branch directly at the interface, but nearby in the matrix (see arrows in Fig. 6c).

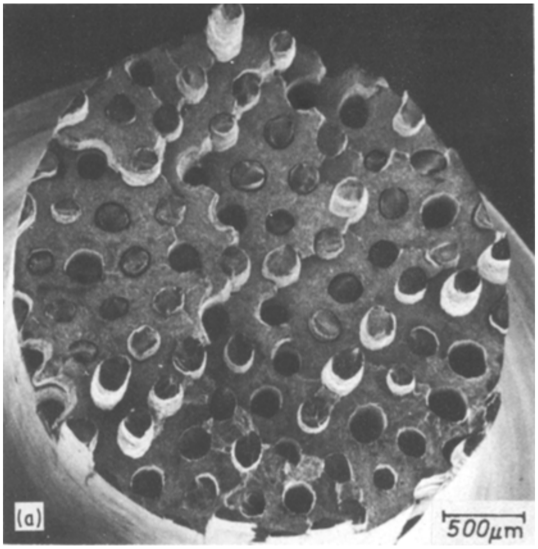

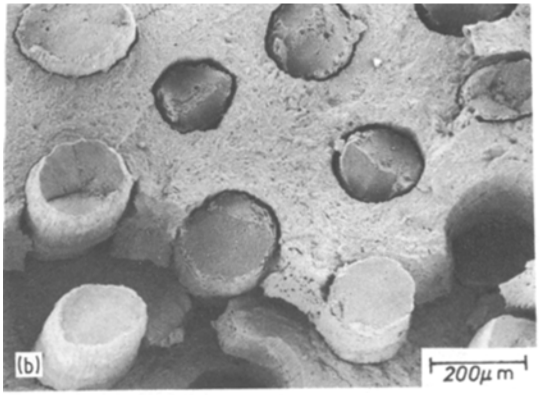

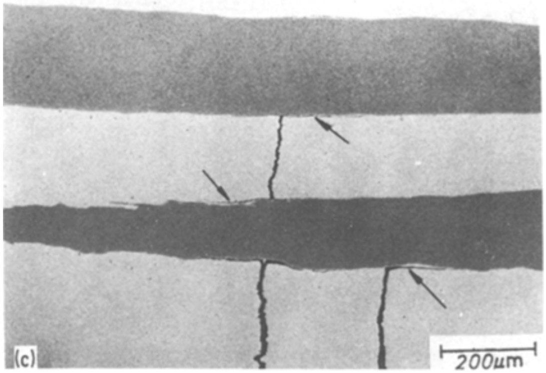

Figure 6 Fatigue behaviour of 80% pre-deformed FRC after matrix recrystallization. (a) Fracture surface; $\Delta\epsilon_{tot} = 2.8 \times 10^{-3}$, $N_f = 8.6 \times 10^7$ cycles; (b) fracture surface of a specimen fatigued for 10^8 cycles at $\Delta\epsilon_{tot} = 2.8 \times 10^{-3}$, and then fractured in a tensile test; (c) longitudinal section of the same specimen as in (b); matrix fatigue cracks branch in the silver matrix near the interface (arrows).

The *in situ* oxidation of the 80% pre-deformed composite (80/Ox condition) results in a similar fatigue behaviour as in the 30/Ox material. The first damage step is the debonding of the interfaces which were weak after the internal oxidation of the fibre surfaces. In addition, at all cyclic strain amplitudes, matrix cracks are generated even earlier than in 80/R samples. Both delamination and early matrix fatigue crack formation prevent the development of the inhomogeneous matrix deformation structure as mentioned in the cases 80/D and 80/R. At the specimen surface the crack-impeding capacity of the reinforcing fibres is again evident. The matrix cracks, as a rule, branch either to neckings or to discontinuities of the surface fibres or advance into the bulk material by by-passing the filaments. At all strain amplitudes the fatigue fracture surfaces macroscopically resemble those of the 80/R FRCs (Fig. 2f). Very high steps in the matrix fracture surface are frequently observed; they may include more than half of the gauge length. Nearly all fibres fail in neckings at various positions with respect to the matrix crack plane. A typical section is shown in Fig. 7.

4. Discussion

Section 4.1 will discuss those parameters which control the development of different fatigue damage modes in the silver–steel FRC and which are also of general importance for metallic fibre composites. In Section 4.2 the effect of the damage and failure mechanism on fatigue life will be considered, and the problem of failure definition

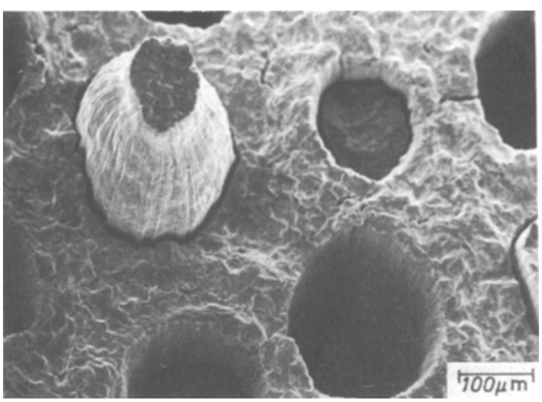

Figure 7 Fatigue fracture surface of 80% pre-deformed FRC with *in situ* oxidized filament surfaces; $\Delta\epsilon_{tot} = 0.8\%$, $N_f = 9 \times 10^3$ cycles.

in such composites will be discussed in Section 4.3.

4.1. Damage development as a result of material condition

The present investigation has revealed two fundamentally different mechanisms of fatigue damage depending on material conditions and load amplitudes:

(a) Failure by formation of only one or very few visible matrix cracks similar to the fatigue behaviour of conventional metallic materials. The damage is restricted mainly to a small region near the final fatigue crack (schematic drawing, Fig. 2a, b and d).

(b) Failure by gradual accumulation of fatigue damage in the matrix and fibre–matrix interface and delayed propagation of the final fatigue crack. Matrix damage is delocalized by spreading into the bulk material (Fig. 2c, e and f).

Near the fatigue limit the material behaviour is mainly determined by the behaviour of a fatigue crack meeting a reinforcing fibre. The following assumptions have been made for a simplified model:

(i) the matrix fatigue crack approaches the reinforcing fibre perpendicular to the fibre (and loading) axis;

(ii) the resulting overload on the filament is reduced linearly along the fibre–matrix interface by means of shear stresses;

(iii) only the main load component in the direction of the fibre axis is considered;

(iv) the interfacial bond strength is constant;

(v) there are no inherent fatigue limit fluctuations in the filament; the fatigue load bearing capacity of the fibres is solely determined by the local fibre cross-section.

The variation of the load amplitude along a reinforcing fibre meeting a matrix fatigue crack is shown schematically in Fig. 8a. Originally, the filament was fatigued with a load amplitude ΔP_n. When approached by the matrix crack the fibre has to take over an additional amount of load. If the total load amplitude exceeds the fatigue limit ΔP_{fl} of the fibre, as in Case 1, fibre failure will be induced by the matrix crack; on the other hand, the fibre will survive in Case 2 where the maximum amplitude ΔP_2^{max} is below ΔP_{fl}. The matrix fatigue crack will stop and then branch at the interface or by-pass the fibre.

The decrease of the stress concentration along the fibre is determined either by the critical shear stress of the matrix τ_m adjacent to the fibre or by the shear strength of the interface τ_i, depending which one is the smaller. The distance x, necessary for complete relaxation of a stress concentration, is assumed to be inversely proportional to τ_i or τ_m. Hence the parameter variations studied in silver–steel FRCs yield the following trends on the fatigue crack propagation mode:

The decrease of the matrix yield strength by recrystallization causes accelerated crack-tip blunting compared to the pre-deformed matrix state and consequently decreases the stress concentration in the reinforcing fibre; in other words, the stress

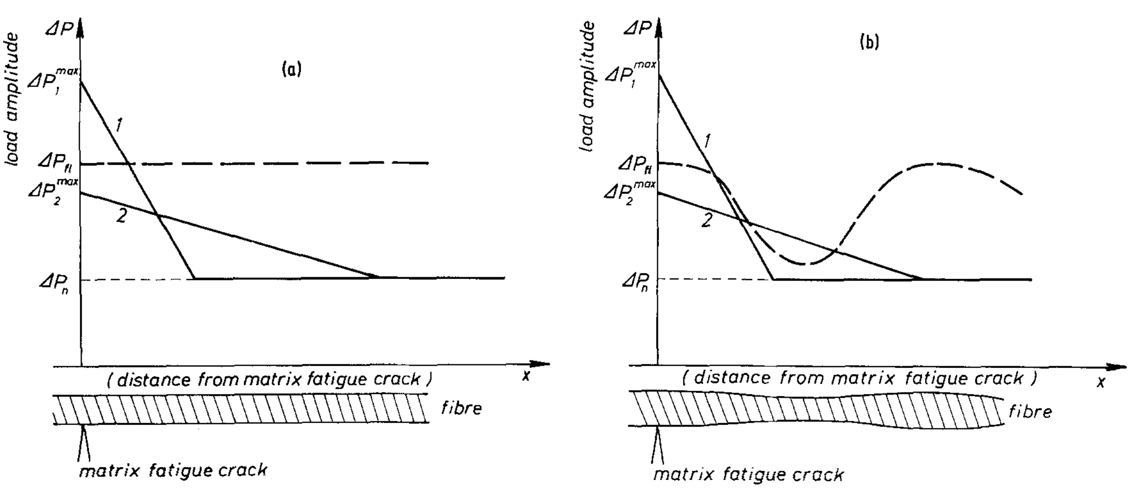

Figure 8 Schematic diagram of the local overload in a reinforcing fibre near a matrix fatigue crack plotted against the distance from the fatigue crack (see text). (a) Fibre with constant fatigue limit ΔP_{fl} (broken line) along its length. (b) fibre with local neck, having an oscillating fatigue limit ΔP_{fl} (broken line) along its length.

concentration following Curve 1 in Fig. 8a changes towards Curve 2: crack branching and delocalization of fatigue damage become more probable. In the 30/R composite, fatigue cracks no longer propagate irrespective of the fibre–matrix interface, even at high load amplitudes (cf. Fig. 1a and b). For the 80/R samples this effect is more obvious (Fig. 6c) and, for example, was confirmed under low-cycle conditions ($\Delta\epsilon_{tot} = 5.2 \times 10^{-3}$) by a gradual decrease of the load amplitude (see Part 1 [1], Fig. 6a).

An increase of the fibre yield strength and fatigue limit given rise to a higher value of ΔP_{fl} in Fig. 8a. Clearly the sensitivity to local stress concentrations is reduced and matrix fatigue cracks can be impeded more efficiently. The difference becomes evident by comparison of the fracture surface micrographs of 30/D (Fig. 1a) and 80/D FRCs (Fig. 5a and b).

Weakening of the fibre matrix interface by *in situ* oxidation of the steel fibre surfaces results in an essential decrease of the stress concentration in the reinforcing filament, generated by an approaching matrix fatigue crack. Corresponding to the relation $x \sim 1/\tau_i$, the additional loading of the reinforcing component is distributed over a longer filament length (Curve 2 in Fig. 8a). Near the fatigue limit the oxide coating prevents filament failure, because fatigue cracks can no longer be induced. Thus gradual matrix crazing develops (Fig. 3).

The effect of one further parameter variation is presented in Fig. 8b: inspired by a study of Cooper [6], experiments were performed to increase the fatigue fracture toughness of silver–steel FRCs by appropriate weak fibre points. Cooper reported that the tensile fracture toughness of FRCs may be raised by such points of weakness; their mutual distance should be less or equal to the critical length of the fibre according to the extent of local fibre weakening. In the present case, points of weakness in the form of multiple fibre necking are due to severe cold forming (80% pre-deformation). Fig. 8b shows the situation when a matrix fatigue crack approaches a "nodal point" of the fibre. The multiple fibre necking yields a tolerable cyclic load amplitude ΔP_{fl}, which oscillates along the fibre axis, according mainly to the local fibre cross-section. The schematic diagram illustrates why most fibre failures occur in the matrix crack plane in the pre-deformed 80/D condition (Curve 1), while the great majority of the fibres fail above or below this plane at points of weakness in FRCs in the 80/R condition (decreased critical shear stress τ_m of the matrix) or in the 80/Ox condition (weakened interfacial shear strength τ_i) (Curve 2). In the first case (Curve 1) the fatigue limit of the filaments is only exceeded near the matrix fatigue crack tip. In the other cases an overload only exists in the adjacent fibre neckings. If the matrix crack does not meet a "nodal" fibre point, the probability of weak-point failure increases. This may be easily reconstructed in Fig. 8b by shifting the oscillating ΔP_{fl} curve to the left.

Hence, points of filament weakness may given rise to an important change of the fatigue crack extension mode by delocalizing the plastic matrix strain at the crack tip, especially after recrystallization of the matrix and/or weakening of the interfacial bond strength. This holds for both low- and high-cycle fatigue. The fatigue crack propagation rate perpendicular to the fibre axis, for example, was observed to be much less in the 80/Ox composite than in the 30/Ox specimens (no multiple necking), heat-treated in the same way. The fatigue fracture surfaces of both materials, too, show fundamental differences (Figs 7 and 1c); the crack path is obviously more expanded in the severely pre-deformed 80/D conditions. Extensive delocalization of damage may occur even in composites with a strong fibre–matrix interfacial bond, for example in the 80/R condition (Fig. 6c).

4.2. The influence of the material condition on the fatigue life

In the following sections some attempts will be made to review the impact of different damage and failure mechanisms on fatigue life and fatigue-related service ability of the present silver–steel FRC and similar metallic composites. This may be done either on a stress-range basis (see Part 1 [1]) or on a strain-range basis. Comparison of tolerable composite stress amplitudes at more than 10^6 cycles to failure with those of the unreinforced matrix normally yields an improved fatigue limit of the matrix*.

For illustration and estimation of "genuine"

*If no essential interactions of the components have to be taken into account during cyclic loading and failure of the weaker matrix immediately leads to composite failure, the fatigue limits of FRC and matrix behave like their Young's moduli.

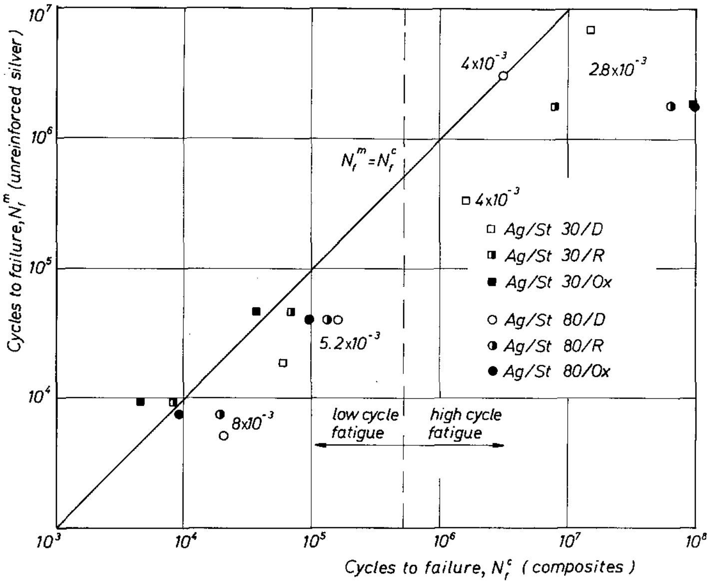

Figure 9 Number of cycles to failure of bulk silver materials plotted against that of FRCs similarly heat treated and always fatigued with identical total strain amplitudes; ($\Delta\epsilon_{tot}$) given in figure (cf. Table I).

composite properties, due to true composite action, it appeared to be more appropriate to compare the numbers of cycles to failure of the FRC and the unreinforced matrix material at comparable total strain amplitudes. It should be kept in mind that the following discussion is performed under this strain-range-based point of view. Such an evaluation is compiled in Fig. 9; results of both low- and high-cycle fatigue are included. The logarithms of the mean numbers of cycles to failure of composites (N_f^c) and correspondingly heat-treated unreinforced silver samples (N_f^m), both loaded by identical strain amplitudes, are plotted against each other. The mean values were evaluated from two to four experiments (see Table I). As long as the silver matrix behaves like unreinforced silver and composite fatigue failure is solely controlled by the matrix, all data points have to coincide with the medial line $N_f^m \equiv N_f^c$. Interactions between the composite components, as described in previous sections, may however result in decisive deviations of the test points from this straight line. An increase in fatigue life of the composites compared to the unreinforced silver matrix (data points are shifted to the right) is either based on a delayed nucleation of those matrix

TABLE I Ultrasonic fatigue results of silver–steel FRC and corresponding silver specimens

Material	Number of specimens	Total strain amplitude, $\Delta\epsilon_{tot}$	Mean number of cycles to failure, $\bar{N}_f$	Remarks on damage mechanism
Composites				
Ag/St 30/D	2	4.0×10^{-3}	1.58×10^6	
Ag/St 30/D	2	2.8×10^{-3}	15×10^6	
Ag/St 30/R	5	2.8×10^{-3}	7.9×10^6	
Ag/St 30/Ox	4	2.8×10^{-3}	100×10^6	No fibre failure*, but several matrix fatigue cracks
Ag/St 30/D	5	4.0×10^{-3}	3.06×10^6	
Ag/St 30/R	6	2.8×10^{-3}	62×10^6	No fibre failure*, but several matrix fatigue cracks
Ag/St 30/Ox	2	2.8×10^{-3}	100×10^6	No fibre failure*, but several matrix fatigue cracks
Unreinforced silver				
Ag 30/D	3	4.0×10^{-3}	0.34×10^6	
Ag 30/D	3	2.8×10^{-3}	6.8×10^6	
Ag 30/R	3	2.8×10^{-3}	1.8×10^6	
Ag 80/D	4	4.0×10^{-3}	3.15×10^6	

*WIth the exception of longitudinally cut surface filaments.

cracks capable of propagating or on an impeded crack extension perpendicular to the load and fibre axis.

In low-cycle fatigue the failure of composites under R and Ox conditions is essentially governed by the matrix properties. Destruction of the brittle oxide films at high strain amplitudes ($\Delta\epsilon_{tot} = 8 \times 10^{-3}$) and the simultaneous formation of notches at the fibre–matrix interface even lead to premature matrix crack nucleation in originally 30/Ox composites compared to unreinforced silver. At such high load amplitudes, plastic deformation and fatigue of the fibres, too, accelerate composite failure.

However, FRCs under 30/D, 80/D and 80/R conditions clearly reveal increased fatigue lives compared to the corresponding bulk silver material. In the D-cases the behaviour can mainly be attributed to a reduced ductility of the silver matrix, while in the 80/R case, the delocalization of damage and impeded fatigue crack propagation is dominant. This was discussed in detail in Part 1 [1].

With decreasing cyclic load amplitude, i.e. under high-cycle fatigue conditions, the macroscopic plastic strain amplitude of the matrix as well as that of the fibres tend to zero. Since delayed formation of fatigue cracks in the low-cycle range can be attributed mainly to a diminished matrix plastic strain amplitude [1], it appears to be quite reasonable that this contribution disappears near the fatigue limit, especially if a severely predeformed matrix is under consideration ($\Delta\epsilon^{m}_{pl} \rightarrow 0$). Consequently, no difference is observed between the number of cycles to failure of 80% pre-deformed silver and corresponding silver–steel composite specimens at $\Delta\epsilon_{tot} = 4.0 \times 10^{-3}$; in materials with only 30% pre-deformation a certain increase of fatigue life is preserved at this cyclic strain amplitude (Fig. 9, Table I).

Simultaneously, the behaviour of matrix fatigue cracks meeting with an interface gains in importance near the fatigue limit. At $\Delta\epsilon_{tot} = 2.8 \times 10^{-3}$, unreinforced, recrystallized silver fails at $N^{m}_{f} = 1.8 \times 10^{6}$; at the same amplitude this value is exceeded by 1 to 2 orders of magnitude in 30/Ox, 80/Ox and 80/R composites (Fig. 9). For low strain amplitudes ($\Delta\epsilon_{tot} = 2.8 \times 10^{-3}$) these material states usually did not show any continuous fatigue crack where both matrix and fibres are fractured at the same time (Table I, right-hand column). On the other hand, extensive mechanical property changes during fatigue were observed in these materials, causing considerable resonant frequency changes and at least the break-down of the ultrasonic fatigue vibration. Subsequent tensile tests often revealed very high residual strengths. For example, an 80/R sample survived 10^{8} cycles at $\Delta\epsilon_{tot} = 2.8 \times 10^{-3}$; the tensile test yielded a remaining ultimate tensile strength of 488 MPa, compared to 523 MPa for a non-fatigued sample. The high remaining strength confirms that the fibres have not been damaged by fatigue, which was also suggested from fractographic observations (Fig. 6b). In addition the matrix, although interspersed by several fatigue cracks, must still take part of the tensile load in order to explain the high remaining strength. Similar results have been previously reported in the case of Al–B FRCs [7].

In materials showing conventional damage behaviour, the breakdown of ultrasonic resonance occurred when a continuous fatigue crack front had spread over a considerable part of the specimen cross-section, fracturing both matrix and fibres.

Disregarding for the moment, problems which are related to the assessment of an appropriate failure criterion of cyclically loaded FRCs, we may conclude the following from the behaviour described: One way to improve the strain-range-based fatigue life of silver–steel fibrous composites under high-cycle fatigue conditions is primarily given by impeded fatigue crack propagation and the resulting delocalization of matrix fatigue damage. High fibre fatigue strength but low matrix critical shear stress, generally speaking, a small τ_m/σ^{f}_{fl} ratio or high fibre fatigue strength and weak interfacial bond, i.e. small τ_i/σ^{f}_{fl} ratio, promote the named failure mode.

As reported in Section 4.1., regularly arranged points of fibre weakness may also contribute to an extension of the fatigue crack path and may also lead to a delocalization of matrix damage. An appropriate co-ordination of the mutual distance and extent of adjacent points of weakness with the matrix strength or the fibre–matrix interfacial bond strength gives rise to an increased fatigue fracture toughness. As a qualitative rule one may keep in mind that the smaller the extent of the weak fibre points and the larger the mutual distance, the lower should be the interfacial bond strength or critical matrix shear strength in order to get an increase in fatigue fracture toughness [8]. Since the introduction of multiple fibre necking in the present study is inevitably associated with an increase of fibre strength (variation of a second parameter) an unambiguous comparison with materials without points of weakness is not available. In particular, it seems to be impossible to answer definitely the question as to whether or not simultaneous maxima of the fatigue limit and fatigue fracture toughness may be achieved by introduction of weak fibre points in the present case or in similar composites. Under tensile test conditions, Cooper [6] did not find such joint maxima of the ultimate tensile strength and the fracture toughness in the resin–phosphor-bronze model composites. In contrast to these results, some independent observations [9, 10] indicate a possible increase of fatigue fracture toughness without loss of fatigue strength: it is reported that a transition from continuous to discontinuous filaments in FRC, in the present case represented by the introduction of multiple fibre necking, affects the ultimate tensile strength rather than the initial part of the tensile stress–strain behaviour, where the reinforcing fibres are still elastic. Fatigue tests, especially those near the fatigue limit, are performed just in this low strain region.

4.3. Definition of failure

The problem of defining an adequate and uniform criterion of failure in FRC has hitherto been omitted in the present study. During low-cycle fatigue, failure was fixed when the composite stress amplitude had dropped to half the value of the initial stress amplitude. For the ultrasonic experiments, the loss of resonance of the system was arbitrarily assumed as the number of cycles to failure. As mentioned above, the latter, according to the material condition, may either signify that a continuous fatigue crack really has fractured a considerable part of the specimen cross-section or that only the matrix and the fibre–matrix interfaces are severely damaged.

Despite the great diversity of microstructural damage mechanisms, different efforts have been made up to now in the literature to define a single efficient and uniform failure criterion for fatigued fibrous composites. One proposal assumed that possible interactions of the composite components should be of minor importance during cyclic loading and that fatigue crack formation in the weaker phase should define the failure of the FRC [11]. This position may underestimate the true fatigue life of metal–metal combinations, especially in composites with high volume-fractions of the reinforcing component. Additionally, an improvement of the fatigue strength of the weaker component on the strain-range basis may only be expected in specific loading regimes ($\sigma_{min}/\sigma_{max} \neq -1$) from the utilization of residual stresses between the components [11–13]. Another proposal defines failure as not occurring before fracture of the second reinforcing component [14]. This definition possibly allows severe crazing of the weaker component and the interfacial region. In practice gradual destruction of the matrix or the filaments frequently results in inadmissible variations of mechanical and other composite properties, such as stiffness, remaining tensile strength, damping behaviour, electrical and thermal conductivity, and so on. Again no universal failure criterion can be found. Hence, the only solution appears to be that proposed by Salkind [15], to define failure according to the projected use of the composite; i.e. different fatigue lifes may be attributed to one and the same material in various applications.

The chance to tailor the damage and fatigue mode of fibrous composites, as described for the silver–steel system, reveals the possibility of changing the material condition according to the projected application; for example: if no property variations of a structural member are allowed, and unexpected failure must not be avoided for security demands, a material will be selected where macroscopic fatigue damage will start as late as possible. In silver–steel composites this is coincident with only local composite damage and relatively quick crack propagation. If, on the other hand, mechanical property changes (except total failure) can be allowed before replacement of the damaged part, a material could be chosen which shows gradual, delocalized damage of one component preceding final failure. In that case, however, one has to take into account that matrix cracks form relatively early.

Adequate material parameters favouring gradual damaging and impeded fatigue crack extension may result in a considerable improvement compared to the unreinforced material under strain-controlled high-cycle fatigue conditions, if fracture of the reinforcing component is a reasonable failure criterion and variations of mechanical and other composite properties are allowed. The main significance of the gradual failure mechanism, however, appears to be the increase of the fatigue fracture toughness, i.e. the chance to guarantee security against unexpected failure of cyclic loaded FRCs and thus reduce inspection requirements.

5. Conclusions

(a) Cyclic loading of unidirectional silver–steel-fibre-reinforced composites under high-cycle fatigue conditions may result in two fundamentally different damage and failure mechanisms and several transitional modes, according to the local stress states arising from matrix fatigue cracks which approach the fibres:

(i) Failure by nucleation and propagation of generally one or few visible matrix cracks similar to the behaviour of conventional metallic materials. The crack-impeding ability of the reinforcing fibres is barely detectable.

(ii) Failure by gradual accumulation of matrix and interfacial fatigue damage and inhibited propagation of the final fatigue crack. Matrix damage is delocalized and spreads into the bulk material.

(b) High matrix strength and strong interfacial bonding, as well as poor fibre strength, give rise to Mechanism (i), whereas low matrix strength or weak interfacial bonding and high fibre strength promote Mechanism (ii).

(c) Multiple necking of the filaments, i.e. points of weakness along each fibre, may also favour gradual damaging and lead to an improvement of the fatigue fracture toughness in silver–steel composites.

(d) To optimize fatigue life under low-cycle fatigue conditions, it is most important to delay matrix fatigue crack formation. Under strain-controlled high-cycle conditions fatigue life can be extended by one to two orders of magnitude if the composite is tailored for gradual damage accumulation, Mechanism (ii), and certain property changes are allowed.

(e) It seems to be unreasonable to provide one single failure criterion for metallic fibre-reinforced composites under cyclic loading conditions. One rather ought to define different failure modes according to the projected application. This may result in the definition of different fatigue lifes or fatigue limits for one and the same material.

References

1. G. ROSENKRANZ, V. GEROLD, D. STÖCKEL and L. TILLMANN, *J. Mater. Sci.* **17** (1981) 264.
2. W. KROMP, K. KROMP, H. BITT, H. LANGER and B. WEISS, in "Ultrasonics International 1973", Conference Proceedings (Science and Technology Press, Guildford, Surrey, 1973) p. 238.
3. L. E. WILLERTZ, *Int. Met. Rev.* **2** (1980) 65.
4. G. ROSENKRANZ, D. STÖCKEL and L. TILLMANN, *Metall* **30** (1976) 645.
5. *Idem, J. Mater. Technol. Test.* **7** (1976) 317.
6. G. A. COOPER, *J. Mater. Sci.* **5** (1970) 645.
7. G. D. MENKE and I. J. TOTH, "Time Dependent Mechanical Behaviour of Composite Materials", AFML-TR-71-102.
8. G. ROSENKRANZ, Thesis, Universität Stuttgart, FRG (1979).
9. B. HARRIS and S. V. RAMANI, *J. Mater. Sci.* **10** (1975) 83.
10. P. TAUTZENBERGER, L. TILLMANN and D. STÖCKEL, *Metall* **32** (1978) 665.
11. G. I. DVORAK and I. Q. TARN, in "Fatigue of Composite Materials", ASTM STP 569 (1975) p. 145.
12. H. J. WEISS, *J. Mater. Sci.* **13** (1978) 1388.
13. G. ROSENKRANZ, *J. Mater. Technol. Test.* **12** (1981) 289.
14. J. R. HANCOCK, in "Composite Materials" Vol. 5: "Fracture and Fatigue", edited by L. J. Broutman, (Academic Press, New York, 1974) p. 371.
15. M. J. SALKIND, in "Composite Materials' Testing and design", ASTM STP 497 (1972) p. 143.

Received 22 May
and accepted 18 June 1981